Computers and Geotechnics 171 (2024) 106385

Contents lists available at ScienceDirect

Computers and Geotechnics

journal homepage: www.elsevier.com/locate/compgeo

Research Paper

A multi-phase/multi-regime modelling approach for saturated granular media

Pietro Marveggio, Matteo Zerbi, Claudio di Prisco *

Politecnico di Milano, Dipartimento di Ingegneria Civile e Ambientale, Piazza Leonardo da Vinci 32, Milano 20132, Italy

A B S T R A C T

When studying, by using continuum-based approaches, liquefaction phenomena, granular flows and granular material reconsolidation, crucial is the correct modelling of the change in material behaviour due to water presence and force chains collapse. To this aim, in this paper, the authors outline a model based on an in-parallel scheme. Three stress contributions are defined: the one associated with force chains applied to the solid skeleton (the effective stress), the one related to particle collisions (dominating for large values of void ratios and when the system is agitated) and the liquid one (not necessarily isotropic for large deviatoric strain rates). The model is conceived to reproduce the material mechanical behaviour of granular media under three different regimes: solid like, fluid like and inertial. The transition from one regime to another, in the model, is governed by the evolution of two state variables: void ratio and granular temperature (a measure of the material agitation). In this paper, the saturated version of the multi-regime model, already conceived for dry granular materials, is proposed. Its capability of reproducing the material fluidization in undrained constant volume rheometer tests is illustrated by discussing the numerical results obtained by using a Material Point Method code.

1. Introduction

Simulating the mechanical behaviour of saturated granular media under general conditions still represents an open challenge in a wide range of geotechnical problems, relative to material liquefaction and reconsolidation. In this perspective, indeed, employing constitutive relationships accounting for grain-grain and liquid-grain interaction mechanisms is crucial. In fact, according to the nature of microstructural interaction occurring in the medium, granular materials behave differently. Under quasi-static conditions, a sand behaves like a solid and can be idealized as a network of long-lasting force chains developing among grains (Calvetti & Emeriault, 1999). Under saturated conditions water can either be still (hydrostatic conditions) or can flow inside the porous medium, being this latter assumed to be still. Alternatively, the entire granular medium flows, large strain rates develop and the same material exhibits a “fluid-like” regime with grains colliding among each other (Calvetti et al., 2019). In this scenario, the grain-grain interaction is affected by the liquid presence, since additional dissipation mechanisms develop. The classic Terzaghi’s effective stress principle, holding in case of quasi static regimes, has to be redefined.

According to the concept of “State of Matter”, matter in the solid state maintains a fixed volume and shape, matter in the liquid state maintains a fixed volume but not shape, while matter in the gaseous state varies in volume and shape. When materials under distinct phases are mixed to each other, like solid grains in air or water, the combined system, that is the resulting mixture, may behave like a solid (solid-like regime), a fluid (fluid-like regime) or a dynamic system (inertial regime). Models capable of dealing with different regimes, combining distinct phases, and simulating the transition processes leading from one regime to another are very rare in the literature, in particular those based on a rigorous thermodynamic interpretation of the mechanical processes occurring in the system.

In case of saturated materials, discrete approaches, accounting for, at the micro scale, grain-grain interactions, can be adopted to tackle this task only if coupled with Computational Fluid Dynamics (CFD) (Leonardi et al., 2014; Tsuji et al., 1993), simulating the role of liquid, also affecting the solid to solid interaction. For the solution of engineering boundary value problems, these approaches require computational costs not compatible with any industrial application. The alternative of disregarding the presence of water, implementing lubrication equivalent forces (Wang et al., 2012; Chèvremont et al., 2020) acting on grains, seems to be reliable only under specific assumptions and under steady conditions (Ness & Sun, 2015).

Investigating at the micro scale the interaction mechanisms under different regimes and during regime transitions and interpreting the system response in a continuum-based framework is not only important

* Corresponding author.
E-mail address: claudio.diprisco@polimi.it (C. di Prisco).

https://doi.org/10.1016/j.compgeo.2024.106385

Available online 7 May 2024

for basic research, but also for many practical applications (for instance, flow-slides or soil-structure interaction when seismic liquefaction occurs).

The approaches proposed in the scientific literature by physicists and hydraulic engineers to simulate the mechanical behaviour of granular media (i) mainly focus on the fluid-like regime, (ii) are formulated under steady conditions, and (iii) interpret the mixture, in case of saturated matters, as a single-phase material (Bingham, 1922; GDR MiDi, 2004; Hunt et al., 2002; Jop et al., 2006). In this community, very popular is the so called μ-e-I rheology (Jop et al., 2006), according to which, under steady simple shear conditions, a relationship between stress level μ, void ratio e and inertial number I exists under dry conditions and has been numerically derived by performing DEM analyses (Chialvo et al., 2012). According to this theory, high values of I correspond to agitated conditions, whereas small I values to quasi-static regimes. More recently, in case of deformable spheres, the e-I relationship has been shown by Redaelli & Di Prisco, 2019 and Redaelli et al., 2021 not to be bijective. To extend the range of applicability of the popular μ-e-I rheology to saturated materials, merging the work of Boyer et al., 2011 and those of Jop et al., 2006, Trulsson et al., 2012 proposed, to account for the liquid viscosity η, the μ-e-I rheology to be modified by introducing a new inertial number K. Again, a unique relation is assumed to exist among K, μ and e. This approach has the advantage of being very simple but shares the same limitations of the original one. Additionally, due to its single-phase formulation, the model cannot fully reproduce the mechanical response of granular materials under static saturated conditions, since does not consider the liquid pore pressure static component (Redaelli et al., 2021).

Alternatively, soil mechanics focuses on the solid-like mechanical behaviour of soils under quasi-static or cyclic loading and, in the geotechnical community, numerous are the constitutive models (Dafalias & Manzari, 2004; Gajo & Muir Wood, 1999) (i) capable of successfully predicting the material response under quasi-static conditions, but (ii) not adequate for simulating granular media when behaving like fluids. In the last decade, some attempts have been done to build a bridge between the two different approaches (Alaei et al., 2021; Baumgarten & Kamrin, 2019; Guo et al., 2021), testifying the interest of the subject in the geotechnical community.

According to the authors, for a correct simulation of the mechanical behaviour of granular media under the different regimes and during the transition from one regime to another, crucial is the thermodynamic comprehension of the dissipative and storing mechanisms developing in the system (Berzi et al., 2011; Vescovi et al., 2013; Redaelli et al., 2016; Marveggio et al., 2022). This is the starting point of the model proposed by the authors, which combines kinetic theory of granular gasses and strain hardening elastic-plasticity. As is the previous versions of the same model, Marveggio et al., 2022 proposed a constitutive framework, based on the introduction of granular temperature (Savage, 1998) as additional state variable, describing the agitation of the granular system.

In this paper, the model is modified to take saturated conditions into account. To this aim, the authors have considered crucial (i) adopting a two-phase mixture (2PM) approach (Soga et al., 2016) and (ii) coupling energetically liquid and solid phases, in agreement with the assumption of the original model.

In this paper the theoretical formulation of the approach is outlined (Section 2), the model hypotheses discussed (Section 3), model predictions at material point level illustrated (Section 4), model implementation in a Material Point Method (MPM) code described (Section 5) and numerical results obtained by simulating constant volume rheometric tests commented (Section 6).

2. 2PM modified formulation

As previously stated, in case of saturated granular materials, a general model formulation accounting for two phases has to be based on the mixture theory (Truesdell & Toupin, 1960), suitable for accounting for interaction between solid and liquid phases. Following this approach, the saturated body can be represented as the superposition of two continua, i.e. solid particles (flowing in case solid fraction experiences a fluid like regime) and pore fluid.

According to mixture theory approach in case of saturated granular media, three field equations are used for both granular and liquid phases (Hutter & Jöhnk, 2004): conservation laws of mass, momentum and energy. In common applications, only the first two equations are employed, whereas the last one disregarded. Due to the thermodynamic nature of the constitutive model proposed by the authors, in the formulation outlined here below, the energy conservation equation cannot be disregarded, since it plays a fundamental role in the solution of the problem and in the description of the evolution of the system.

For the granular phase, identified by the subscript G, the mass balance reads:

$$\frac{D}{Dt}\frac{1}{1+e}\rho_P+\rho_P\nabla\bullet\frac{1}{1+e}\boldsymbol{u}_G=0 \tag{1}$$

where $\boldsymbol{u}_G$ is the local mean velocity vector of the granular phase ($\boldsymbol{u}_G = \langle \boldsymbol{u}_p \rangle$, where $\langle\rangle$ represents average at the Representative Elementary Volume (REV) scale and $\boldsymbol{u}_p$ the single grain particle velocity vector), ρ_P the solid density and e the void ratio. Moreover, $\frac{D}{Dt}$ denotes the material derivative and is defined as:

$$\frac{D}{Dt}=\frac{\partial}{\partial t}+\boldsymbol{u}\bullet\nabla \tag{2}$$

where $\frac{\partial}{\partial t}$ is the local time derivative, $\boldsymbol{u}$ the velocity vector and ∇ the nabla operator.

Concerning the liquid phase, identified by subscript L, the mass balance, disregarding any rate of mass growth term, reads:

$$\frac{D}{Dt}\frac{e}{1+e}\rho_L+\rho_L\nabla\bullet\frac{e}{1+e}\boldsymbol{u}_L=0 \tag{3}$$

where ρ_L is the liquid density and $\boldsymbol{u}_L$ is its velocity field vector.

Considering gravity as the only source of external body load, the momentum balance equation for the granular phase is given by:

$$\frac{1}{1+e}\rho_P\frac{D\boldsymbol{u}_G}{Dt}+\nabla\bullet\boldsymbol{\sigma}_G+\boldsymbol{B}+\boldsymbol{F}-\frac{1}{1+e}\rho_P\boldsymbol{g}=0 \tag{4}$$

while the one related to the liquid phase reads:

$$\frac{e}{1+e}\rho_L\frac{D\boldsymbol{u}_L}{Dt}+\nabla\bullet\boldsymbol{\sigma}_L-\boldsymbol{B}-\boldsymbol{F}-\frac{e}{1+e}\rho_L\boldsymbol{g}=0 \tag{5}$$

In Equations (4) and (5), $\boldsymbol{F}$ stands for the interaction force vector between the two phases, and depends mainly on the relative velocity between the two phases ($\boldsymbol{u}_G-\boldsymbol{u}_L$, i.e. the drag force), while $\boldsymbol{g}$ is the gravity acceleration vector, whereas $\mathbf{B}$ stands for a buoyancy vectorial term, defined as:

$$\boldsymbol{B}=\frac{1}{1+e}\nabla\bullet\boldsymbol{\sigma}_L-\nabla\frac{1}{1+e}\boldsymbol{\sigma}_L \tag{6}$$

In Equations (4) and (5) $\boldsymbol{\sigma}_G$ and $\boldsymbol{\sigma}_L$ are the stress tensors of the granular and liquid phase, respectively (the definition of such a buoyancy term overrides the eventual requirement of partial stress definition). The two stress contributions work in parallel:

$$\boldsymbol{\sigma}=\boldsymbol{\sigma}_G+\boldsymbol{\sigma}_L \tag{7}$$

If one disregards relative motion among the two phases, so that the macroscopic velocity of the liquid phase is assumed to coincide with that of the granular one ($\boldsymbol{u}=\boldsymbol{u}_G=\boldsymbol{u}_L$), $\boldsymbol{F}$ in Equations (4) and (5) vanishes.

Finally, the energy balance for the granular phase, disregarding any exchange of energy due to exchange of mass, is assumed by the authors as:

$$\frac{1}{1+e}\rho_P\frac{DE_G}{Dt}+\nabla\bullet(\boldsymbol{\sigma}_G\bullet\boldsymbol{u}_G)+\nabla\bullet\boldsymbol{q}_G+\Gamma_G+\Lambda+\boldsymbol{B}\bullet\boldsymbol{u}_G+\boldsymbol{F}\bullet\boldsymbol{u}_G-\frac{1}{1+e}\rho_G\boldsymbol{g}\bullet\boldsymbol{u}_G=0 \tag{8}$$

A similar equation can be exploited for the fluid phase:

$$\frac{e}{1+e}\rho_L\frac{DE_L}{Dt}+\nabla\bullet(\boldsymbol{\sigma}_L\bullet\boldsymbol{u}_L)+\nabla\bullet\boldsymbol{q}_L+\Gamma_L-\Lambda-\boldsymbol{B}\bullet\boldsymbol{u}_L-\boldsymbol{F}\bullet\boldsymbol{u}_L-\frac{e}{1+e}\rho_L\boldsymbol{g}\bullet\boldsymbol{u}_L=0 \tag{9}$$

In Equations (8) and (9), E_G and E_L are the internal specific energies stored in granular and liquid phases, respectively, $\boldsymbol{q}_G$ and $\boldsymbol{q}_L$ stand for the fluxes of energy vectors, while their divergence represents the energy diffused by the granular and liquid phases, respectively. Finally, Γ_G and Γ_L, always non negative, are the rate of energy dissipation of granular and liquid phases, whereas Λ, according to the authors, is the rate of energy that the granular phase exchanges, due to microscale interactions, with the liquid one.

As is suggested by Marveggio et al. (2022):

$$E_G=E_{G,E}+E_{G,k}+E_{G,h} \tag{10}$$

where $E_{G,E}$ are the elastic stored, $E_{G,k}$ the specific kinetic and $E_{G,h}$ the thermal energies, respectively. The specific thermal energy $E_{G,h}$, in case of granular flows, according to Jaeger et al., 1996 and Aranson & Tsimring, 2006, is at least ten orders of magnitude lower than both $E_{G,E}$ and $E_{G,k}$. Here below athermal materials are considered, so that:

$$E_G=E_{G,k}+E_{G,E} \tag{11}$$

$E_{G,E}$ is defined by the authors as:

$$E_{G,E}=E^{FC}_{G,E}+E^{COL}_{G,E}, \tag{12}$$

being $E^{FC}_{G,E}$ the elastic energy stored by force chains and $E^{COL}_{G,E}$ the collisional elastic energy. Such a distinction, for the sake of simplicity, can be done once the dynamic interaction characteristic time duration (t_c) is computed: $E^{COL}_{G,E}$ is the elastic energy stored by all the particles experiencing collisions, that is interactions characterized by a force fluctuation period equal to t_c.

According to Savage (Savage, 1998):

$$E_{G,k}=\frac{1}{2}\rho_G\frac{1}{1+e}\langle|\boldsymbol{u_p}\bullet\boldsymbol{u_p}|\rangle \tag{13}$$

or:

$$E_{G,k}=E^M_{G,k}+E^F_{G,k}=\frac{1}{2}\rho_G\frac{1}{1+e}|\boldsymbol{u}_G\bullet\boldsymbol{u}_G|+\frac{3}{2}\rho_G\frac{1}{1+e}T. \tag{14}$$

where $E^M_{G,k}$ is the REV kinetic energy, $E^F_{G,k}$ the fluctuating kinetic energy, T the granular temperature (Savage, 1998):

$$T=\frac{1}{3}\langle|\check{\boldsymbol{u}}_P\bullet\check{\boldsymbol{u}}_P|\rangle \tag{15}$$

whereas:

$$\check{\boldsymbol{u}}_P=\boldsymbol{u}_P-\boldsymbol{u}_G \tag{16}$$

Finally, by linearly combining Equations (8) with the vector product of $\boldsymbol{u}_G$ by Equations (4), and by assuming $\boldsymbol{\sigma}_G$ to be a symmetric tensor, we obtain:

$$\frac{1}{1+e}\rho_P\frac{D\left(E^F_{G,k}+E_{G,E}\right)}{Dt}-\boldsymbol{\sigma}_G:\dot{\varepsilon}_G+\nabla\bullet\boldsymbol{q}_G+\Gamma_G+\Lambda=0 \tag{17}$$

where $\dot{\varepsilon}_G$ is the strain rate tensor of the granular phase, defined as the symmetric part of the gradient of $-\boldsymbol{u}_G$.

According to the so called parallel scheme (Berzi et al., 2011; Marveggio et al., 2022; Redaelli et al., 2016; Vescovi et al., 2013), Γ_G is assumed to be the sum of two contributions:

$$\Gamma_G=\Gamma_{FC}+\Gamma_{COL} \tag{18}$$

where Γ_{FC} is the rate at which energy is dissipated by enduring contacts, and Γ_{COL} the energy dissipated by collisions.

Analogously:

$$\sigma_G=\sigma_{FC}+\sigma_{COL} \tag{19}$$

where subscripts "FC" and "COL" stand for "force chains" and "collisional", respectively. When the first term of Equation (19) prevails, the granular material is assumed to behave like a solid (quasi-static regime). On the other hand, when σ_{COL} prevails, a stable contact network cannot develop and particles interact mainly by means of collisions. In this case, the material response can be assimilated to that of a fluid (collisional regime).

Analogously, the flux of energy $\boldsymbol{q}_G$ is written as:

$$\mathbf{q}_G=\mathbf{q}_{FC}+\mathbf{q}_{COL} \tag{20}$$

where $\mathbf{q}_{FC}$ is related to development/collapse of force chains, characterized by the mesoscale internal length (Clerc et al., 2021) whereas $\mathbf{q}_{COL}$ is associated with the fluctuating energy propagation, due to the particle kinetic energy locally transmitted at contacts, prevailing in the collisional regime.

By substituting Equations (18), 19 and 20 in Equation (17) and by assuming Λ to be exchanged with the colliding particles only:

$$\frac{1}{1+e}\rho_P\frac{D\left(E^{COL}_{G,E}+E^{COL}_{G,k}\right)}{Dt}-\boldsymbol{\sigma}_{COL}:\dot{\varepsilon}_G+\nabla\bullet\boldsymbol{q}_{COL}+\Gamma_{COL}+\Lambda=0 \tag{21}$$

$$\frac{1}{1+e}\rho_P\frac{D\left(E^{FC}_{G,E}\right)}{Dt}-\boldsymbol{\sigma}_{FC}:\dot{\varepsilon}_G+\nabla\bullet\boldsymbol{q}_{FC}+\Gamma_{FC}=0. \tag{22}$$

The term $\nabla\bullet\boldsymbol{q}_{FC}$, representing the divergence of the flux of energy associated with the microstructural rearrangement of the solid skeleton, describes the non-locality of the quasi-static constitutive relationship (Aifantis, 1992; De Borst & Mühlhaus, 1992), interpreted according to gradient theory.

As far as the liquid phase is concerned, analogously to what done for the granular phase, by linearly combining Equation (9) with the vector product of $\boldsymbol{u}_L$ by Equations (5), and by assuming $\boldsymbol{\sigma}_L$ to be a symmetric tensor, we obtain:

$$\frac{e}{1+e}\rho_L\frac{DE_L}{Dt}-\boldsymbol{\sigma}_L:\dot{\boldsymbol{\varepsilon}}_L+\Gamma_L-\Lambda=0. \tag{23}$$

3. Constitutive modelling

The main objective of multi-regime models consists in simulating the regime transition taking place in granular materials for large changes in both void ratio and strain rate. As was previously mentioned, the model by Marveggio et al., (2022) employees thermodynamics to describe the mechanical processes justifying fluidization/reconsolidation of granular assemblies under dry conditions. In particular, according to the model, when the granular phase behaves like a solid, E_G is mainly stored elastically (in force chains $E^{FC}_{G,E}$), whereas when behaves like a fluid, E_G is mainly stored as fluctuating energy ($E^{COL}_{G,E}+E^{COL}_{G,k}$). When the material is saturated, crucial is the description of the mechanisms responsible of the energy exchange between granular and liquid phases.

In this perspective, an extension of effective stress principle to fluidized conditions is mandatory (Marveggio et al., 2023), since under these conditions Γ_L is of the same order of magnitude of Γ_G (in this case coinciding with Γ_{COL}):

$$\boldsymbol{\sigma}' = \boldsymbol{\sigma}_{FC} = \boldsymbol{\sigma} - \boldsymbol{\sigma}_{COL} - \boldsymbol{\sigma}_L \tag{24}$$

where both $\boldsymbol{\sigma}_{COL}$ and $\boldsymbol{\sigma}_L$ are characterized by a not nil deviator.

In this section, the main hypotheses of the model are briefly summarized, but, for the sake of brevity, constitutive relationship equations are omitted. In Subsection 3.2, as far as the liquid phase is concerned, the expression employed by the authors for $\boldsymbol{F}$ as well as a synthetic expression for $\boldsymbol{\sigma}_L$ are reported.

3.1. Granular contributions

In Marveggio et al. (2022), the collisional contribution ($\boldsymbol{\sigma}_{COL}$ in Equation (20) is obtained by adopting modified kinetic theories of granular gases (Berzi & Jenkins, 2015; Campbell, 2006; Garzó & Dufty, 1999; Jenkins & Savage, 1983; Lun, 1991), in case of frictional and deformable particles. These theories do not account for angular momentum and fluctuating energy associated with rotational granular temperature but, to account for their effects, propose (Jenkins & Zhang, 2002) to modify the coefficient of restitution.

They assume (i) for $\boldsymbol{\sigma}_{COL}$ a nonlinear dependence on e, T and $\dot{\varepsilon}_{ij}$, (ii) e evolving according to Equation (1) and (iii) T with Equation (21). Any increase in T at constant e and any decrease in e at constant T cause an increase in both $\boldsymbol{\sigma}_{COL}$ and stress ratio. According to modified kinetic theories, at steady state, once e and deviatoric strain rate tensor are assigned, state of stress and T can be derived. According to Redaelli & di Prisco (2019), for $T \rightarrow 0$, this steady state tends to the well-known critical stationary state. Such an hypothesis is fundamental for conceiving a coherent in-parallel constitutive model. The additional term Λ in Equation (21) (Subsection 3.2), representing the exchange in energy between granular and liquid phases, describes the influence of pore water in affecting the collisional mechanical response: this additional dissipating term, reducing the T value, affects $\boldsymbol{\sigma}_{col}$. The expressions chosen for $E^{COL}_{G,E}$, $E^{F}_{G,k}$, $\boldsymbol{\sigma}_{COL}$, $\boldsymbol{q}_{COL}$ and Γ_{COL} (Equation (21) are fully detailed in Marveggio et al. (2022).

As far as the force chains related term is concerned ($\boldsymbol{\sigma}_{FC}$ in Equation (22), a local ($\boldsymbol{q}_{FC} = 0$) quasi-static rate-independent elastic–plastic constitutive relationship with an anisotropic strain hardening is employed (Marveggio et al., 2022). Even in this case, fundamental is the definition of the critical state locus, employed in the model as an attractor. With respect to the original formulation proposed by Marveggio et al., 2022, as was already done in Marveggio et al. (submitted), the critical state locus shape in the deviatoric plane is here assumed to coincide with Lade-Duncan, instead of Matsuoka-Nakai, criterion. Dilatancy is assumed not to depend on α_σ (Lode angle) and to be governed by a function depending on both void ratio and stress level, nullifying when critical state locus is reached, whereas in the deviatoric plane the flow rule is associated.

The size of the closed shaped yield locus (Nova, 1988; di Prisco et al., 1993) is ruled by a hardening variable r_c. The complete fluidization of the material, corresponding to the nullification of enduring contacts, is described by the nullification of r_c. Indeed, from a thermodynamic point of view, the yield locus size is a measure of the energy that force chains may store elastically. According to the model, r_c reduces for negative values of $\dot{\varepsilon}^{vol}_{pl}$ (where $\dot{\varepsilon}^{vol}_{pl}$ is the volumetric contribution of the plastic strain rate tensor $\dot{\boldsymbol{\varepsilon}}_{pl}$). The nullification of r_c may take place, for instance, independently of the imposed strain rate, during constant volume tests, if the imposed void ratio is sufficiently large (loose conditions), or, during constant pressure tests, independently of the initial void ratio, if the strain rate imposed is sufficiently high. In this latter case the increase in T, owing to the in-parallel scheme (Eq. (18)), indirectly causes a negative value for $\dot{\varepsilon}^{vol}_{pl}$.

To account for strain-induced anisotropy, the axis $\boldsymbol{\chi}$ (a back-stress second order tensor) of the yield function is assumed to rotate. $\boldsymbol{\chi}$ describes at the macro scale the directional characteristics of the micro structure and, for large deviatoric strains, tends to $\widehat{\boldsymbol{\chi}}$, assigned this latter for any α_σ. When fluidization takes place r_c nullifies but $\boldsymbol{\chi}$ stops evolving. According to this hypothesis, supported by numerical DEM results (Redaelli & di Prisco, 2021), the directionality of the microstructure is not erased by solid skeleton disruption, since even grain collisions are not disordered but aligned in agreement with the strain rate imposed.

3.2. Liquid contribution

Under saturated conditions, the presence of water gives rise to two additional dissipative terms (Equations (7) and (8): term $-\boldsymbol{F} \bullet (\boldsymbol{u}_L - \boldsymbol{u}_G)$ represents the dissipation of energy associated with drag forces and with a difference in the mean value of the two phase velocities, Γ_L is the dissipation term surviving even if $\boldsymbol{u}_G = \boldsymbol{u}_L$, associated with (i) $\dot{\boldsymbol{\varepsilon}}_L$, (ii) $\check{\boldsymbol{u}}_P$ and (iii) the fluctuating velocity of water.

The authors adopt the following expression for the drag force:

$$\boldsymbol{F} = -\frac{\eta_0}{\kappa_L}\frac{e}{1+e}(\boldsymbol{u}_L - \boldsymbol{u}_G), \tag{25}$$

where η_0 is the liquid molecular viscosity, while κ_L the solid intrinsic permeability, computed and updated as a function of the void ratio according to (Ergun, 1952):

$$\kappa_L = A^2 d^2 \left[180\frac{1}{e^2} + 18\frac{e^2}{(1+e)^3}\left(1 + 1.5\sqrt{\frac{1}{1+e}}\right)\right]^{-1}, \tag{26}$$

where A is a sphericity parameter (equal to 1 in case of ideal assemblies of spheres) and d the particle diameter.

According to Equation (23), Γ_L may be evaluated once $\boldsymbol{\sigma}_L$ and Λ are defined.

In the model employed by the authors: $\boldsymbol{\sigma}_L$ is assumed to linearly depend on the deviatoric part of $\dot{\boldsymbol{\varepsilon}}_L$:

$$\boldsymbol{\sigma}_L = u_w \boldsymbol{I} + 2\eta \dot{\boldsymbol{\varepsilon}}^d_L, \tag{27}$$

where u_w is the isotropic pore pressure, depending on liquid mass and linear momentum balances, but not on the liquid volume (the liquid is assumed to be incompressible), nor on the granular phase agitation, η is the macroscopic viscosity, assumed to be isotropic and not coinciding with the liquid molecular viscosity η_0, whereas Λ is expected to be defined as a function of T, since it represents the part of fluctuating energy of grains transferred to the liquid, and there dissipated.

$\eta \neq \eta_0$, since the presence of immersed grains produces three effects:

(i) the liquid streamlines deviation from their original path in proximity of grains;
(ii) the lubrication effect, occurring when two or more particles approach each other and the liquid in the region in between is squeezed out, due to the increase in its local pressure;
(iii) the water damping of granular fluctuating motion.

$\eta - \eta_0$ represents, therefore, a liquid-granular coupling term and is assumed to depend on e only, since turbulences are disregarded. The liquid mechanical response is assumed to be isotropic and Newtonian, with η only depending on void ratio, as in Vescovi et al. (2020).

As was previously mentioned, Λ is expected to be defined as a function of T since it represents the part of fluctuating energy of grains transferred to the liquid, and there dissipated. Since the dissipation approach defined in Vescovi et al. (2020) for steady simple shear

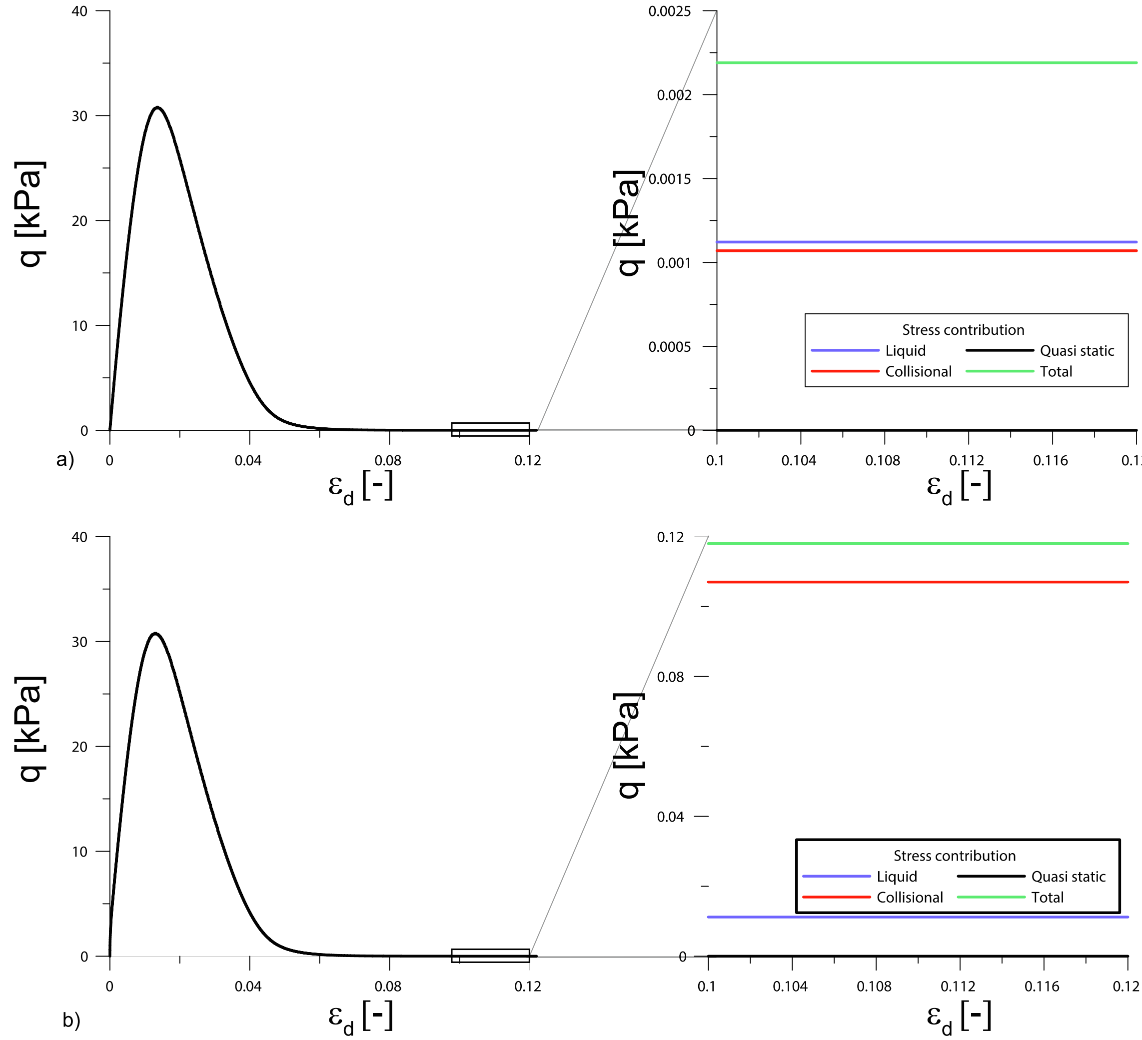

Fig. 1. Undrained standard triaxial compression test results: a)$\dot{\varepsilon}_d = 1\ s^{-1}$, b)$\dot{\varepsilon}_d = 10\ s^{-1}$.

conditions holds also in evolving and general condition, also the expression of Λ coincides.

4. Model discussion: undrained triaxial test results

In this section, at the REV scale, the capability of the model of reproducing regime transition is illustrated. In particular, two undrained standard triaxial compression tests on fully saturated loose sand specimens are numerically simulated. Both specimens are characterized by an initial void ratio $e_0 = 0.70$, an initial isotropic consolidation of 50 kPa and an initial pore water pressure of 50 kPa. The constitutive parameters employed are taken from Marveggio et al (2022). Two different deviatoric strain rates are imposed: $\dot{\varepsilon}_d = 1\ s^{-1}$ and $\dot{\varepsilon}_d = 10\ s^{-1}$.

In Fig. 1, the numerical results, obtained by imposing $\dot{\varepsilon}_d = 1\ s^{-1}$ (Fig. 1a) and $\dot{\varepsilon}_d = 10\ s^{-1}$ (Fig. 1b), are plotted in the deviatoric stress q versus deviatoric strain plane. The (i) quasi-static, (ii) collisional and (iii) liquid q contributions are made explicit in the $0.10 < \varepsilon_d < 0.12$ range (note that axis scales are also magnified). Initially, the mechanical response is almost entirely dominated by the quasi-static contribution. As a matter of fact, the two curves of Fig. 1a and 1b practically coincide. For $\varepsilon_d > 0.05$, the quasi-static contribution (black line in Fig. 1) becomes nil due to the material fluidization. The residual deviatoric stress (green line), orders of magnitude smaller, is given by the sum of collisional (red line) and water (blue line) contributions. For $\dot{\varepsilon}_d = 1\ s^{-1}$ (Fig. 1a), the two contributions are almost equivalent (Newtonian regime, that is $q \propto \dot{\gamma}$), while for $\dot{\varepsilon}_d = 10\ s^{-1}$ (Fig. 1b) the collisional one is dominating (Bagnoldian regime, that is $q \propto \dot{\gamma}^2$) and the residual value of q is two orders of magnitude larger.

A more detailed description of the results obtained by using this model under drained conditions are in Marveggio et al., (2022, 2023, s. d.).

5. Numerical implementation in a MPM code

The constitutive model has been implemented in the open-source dynamic explicit MPM code ANURA3D, a software developed since 2008 to numerically simulate large deformations and soil–water–structure interaction problems (ANURA 3D, 2023).

The Material Point Method extends the traditional solution scheme of a Finite Element Method (FEM), allowing material points (MPs), acting as Lagrangian integration points and in which the material mass is lumped, to flow within a fixed Eulerian mesh, discretizing this latter spatial domain.

In Marveggio et al. (submitted), the dry version of the constitutive model was implemented adopting a single point formulation (Fern et al., 2019). In this paper, two distinct sets of MPs are instead used for the material discretization. According to the authors, when regime transition takes place and phase separation is expected, the use of the double point formulation according to mixture theory, although more computational consuming (Fern et al., 2019), is mandatory. Each phase, separately represented by two different sets of Lagrangian MPs, moves

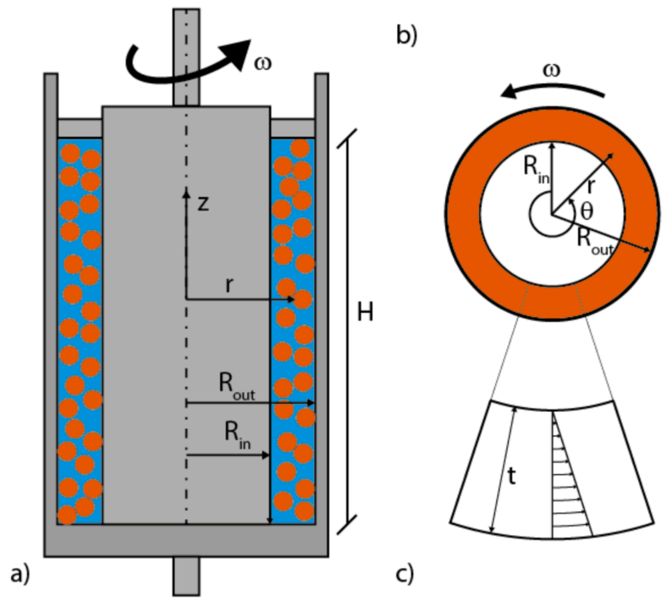

Fig. 2. Scheme of performed rheometer tests: a) front and b) above views and c) steady state imposed velocity profile.

Table 1
List of micro-mechanical input data for the constitutive model.

ρ_p [kg/m^3]	d_p [m]	E_p [MPa]	μ_p [−]	ε_n [−]
2600	0.002	300	0.3	1

Table 2
List of calibrated constitutive model parameters governing the collisional response.

e_m [−]	e_{cc} [−]	e_{ce} [−]
1.5	0.715	0.73

independently and its mass remain constant: the conservation of both solid and liquid mass is a priori satisfied (Fern et al., 2019). On the other hand, the linear momentum balance is enforced separately on the two phases, by considering buoyancy and drag interactions (Fern et al., 2019).

Due to the constitutive model formulation assumptions, only the energy balance associated with collisional terms and their coupling due to the liquid presence must be solved (Eq. (7)). To this aim, as was in Marveggio et al., (submitted), T is added as a material variable to the solid MPs only. T is linearly mapped to the node for the MPM solution scheme, while, as is done for linear momentum balance, a forward Euler approach is used for time integration during the core FEM-like solution scheme. For the sake of stability, the remap procedure from nodes to MPs is obtained by referring to mass-averaged quantity, as it is done in ANURA3D also for node to MP velocity remapping procedure which refers to momentum transfer. The convergence to the numerical solution is obtained by a suitable combination in terms of time discretization (due to the explicit nature of the integrating algorithm), mesh refinement and material points discretization (Wilson et al., 2021).

Table 4
Test IDs with imposed final tangential velocity.

ID test	$\bar{v}_\theta^{max}$ [m/s]
1	0.033
2	0.33
3	3.3

6. MPM numerical simulation of undrained constant volume rheometer tests

In this section, the previously mentioned ANURA3D numerical code, in which the multi-regime model is implemented, is employed to simulate the mechanical response of a saturated loose sand (initial void ratio $e_o = 0.818$) tested in a rheometer ($R_{in} = 0.08m$, $R_{out} = 0.11m$) at constant volume and under undrained conditions (Fig. 2a). The total volume of the mixture (water plus solid fraction) as well as fluid and solid masses are imposed to be constant during the test. The constitutive parameters employed are listed in Tables 1, 2 and 3, and $\eta_0 = 0.001 Pa \bullet s$, since the material is saturated with water. The test is performed by imposing a velocity to the outer ring of the apparatus (Fig. 2b) and by keeping zero the inner ring velocity. Owing to the symmetry of the boundary conditions imposed, the problem is numerically solved under plane strain conditions ($\varepsilon_z = \dot{\varepsilon}_z = 0$). The test is characterized by three phases: (i) under drained condition the specimen is initially isotropically consolidated (in this phase external lateral walls are substituted by a static condition, $\dot{\sigma}_r = \dot{\sigma}_z$), (ii) subsequently both external lateral and upper static conditions are substituted by kinematic constrains ($v_r(r = R_{out}) = 0$, $v_z = 0$) and $v_\theta(r = R_{out}) = \bar{v}_\theta(t) = a \bullet t$, where a is a constant defining the outer ring acceleration, (iii) $v_r(r = R_{out}) = v_z = 0$, $\bar{v}_\theta(t) = \bar{v}_\theta^{max}$. Here in the following, different $\bar{v}_\theta^{max}$ values and one $a = 333 \frac{m}{s^2}$ are considered (Table 4). The results shown in Figs. 3-6 concern phases (ii) and (iii).

Since the volume of the specimen, solid and water masses are imposed to be constant and water almost incompressible (real liquid stiffness is used in the code), during the test the pore water pressure remains constant. Nevertheless, when the material fluidizes (analogously to what already illustrated in Section 4), the presence of water is fundamental in affecting the mechanical behaviour of the mixture, since the water dissipates energy and influences the evolution of granular temperature.

From a macroscopic point of view, in Fig. 3, the material fluidization is illustrated in terms of (i) solid fraction stress path (shear stress $\bar{\tau}$ vs normal stress $\bar{\sigma}_G$, calculated by averaging along θ and r), (ii) $\bar{\tau}$-$\bar{\gamma}$ (where $\bar{\gamma}$ is the shear strain, averaged along θ and r), (iii) final values of $\bar{\tau}$ and averaged shear strain rate $\dot{\bar{\gamma}}$ (the three points refer to the three tests of Fig. 3a and 3b). In Fig. 3a and 3b the peak in $\bar{\tau}$ and the strong reduction in both $\bar{\tau}$ and $\bar{\sigma}_G$, testifying the material fluidization, are evident. Apparently, the radial velocity imposed slightly affects the numerical results. The dependence of $\bar{\tau}$ on the velocity imposed at steady conditions is instead evident in Fig. 3c: the increasing trend is due to the role of granular temperature.

The numerical results allow also to describe both the distribution of strains within the numerical specimen and the specimen homogeneity. For the sake of brevity, only numerical results concerning tests 1 and 3 (Table 4) are illustrated. As is evident in Fig. 4, the value of γ along r (the values of γ are averaged along θ and represented for four time instants in test 1 and three time instants in test 3) is not constant, as was expected in case of uniformity. Initially, strains mainly develop in the inner zone

Table 3
List of calibrated constitutive model parameters governing the strain hardening plastic response.

β [−]	γ [−]	δ_1 [−]	δ_2 [−]	θ_{cc} [−]	θ_{ec} [−]	θ_ψ [−]	c_{pc} [−]	$c_{p\psi}$ [−]	B_p [−]	ξ_ψ [−]	a [−]
0.5	4.1	1	0.8	0.157	0.201	0.5	15	10	0.001	1.75	0.178

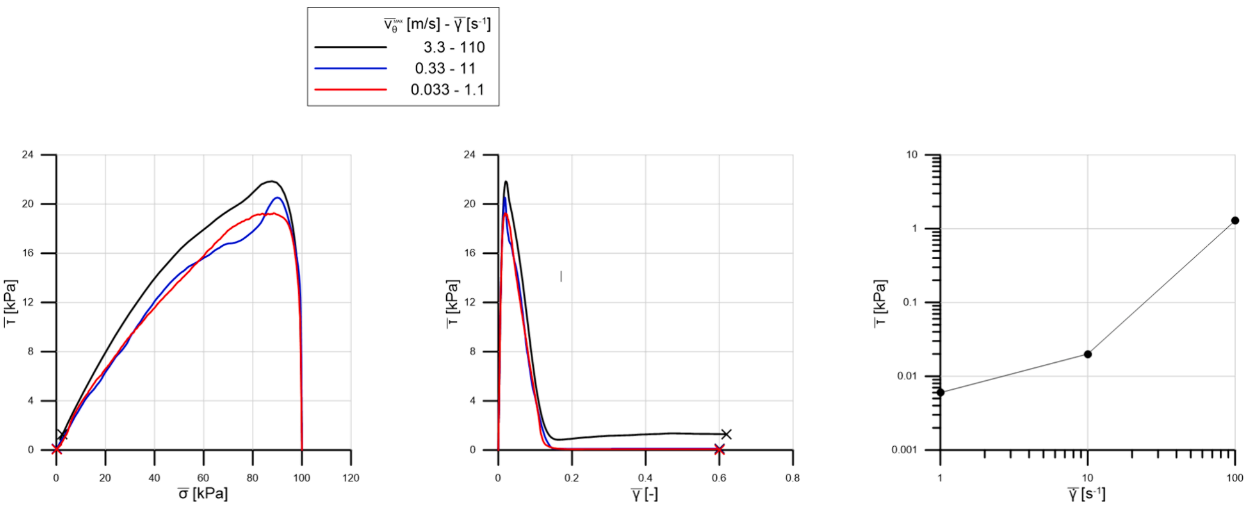

Fig. 3. Tests 1–3: averaged quantities measured during the test in a) $\overline{\tau}-\overline{\sigma}$ and b) $\overline{\tau}-\overline{\gamma}$ planes and steady-state measurements in $\overline{\tau}-\dot{\gamma}$ plane.

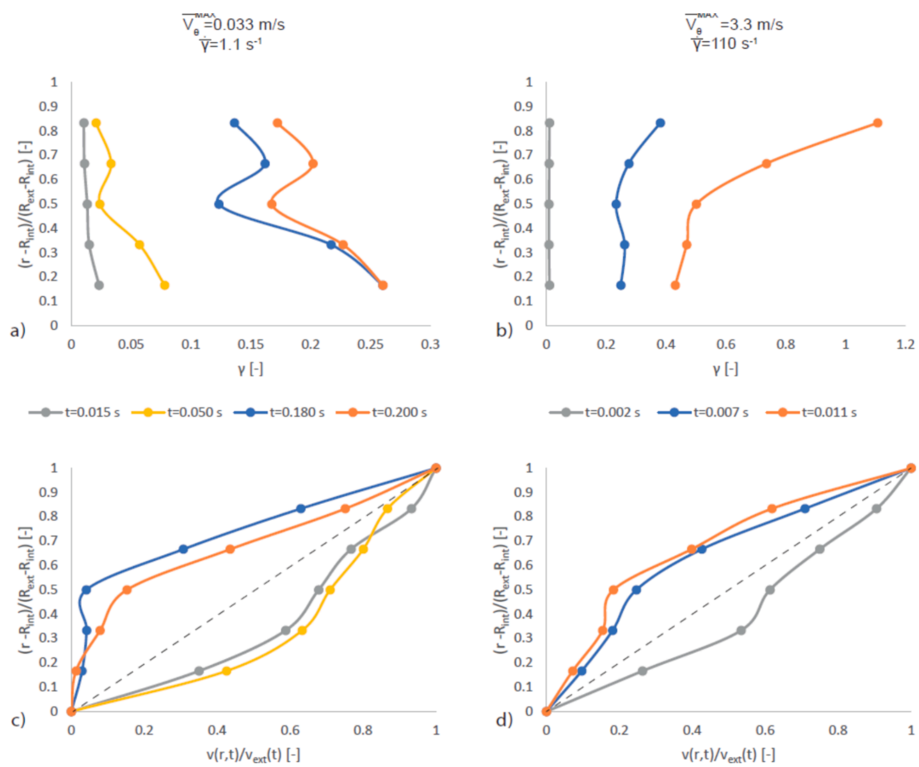

Fig. 4. Test 1 and 3: radial distribution of shear strain (a, b) and velocity (c, d) for different instants of time. Dashed line indicates the ideal velocity profile in case of uniform velocity distribution.

(grey and yellow lines in Fig. 4a, and grey line in Fig. 4b), whereas subsequently shear strain rate mainly develop in the external zone. This mechanism takes place since initially the material behaves like a solid and deforms mainly in the inner zone, where, due to the radial geometry, shear stresses are larger; subsequently, the material behaves like a fluid and the energy provided to the system by the external ring motion is mainly dissipated by the external zone of the numerical specimen.

Fluidization in the specimen is therefore testified by the velocity distribution along r (Fig. 4c) changing with time. Although for different time instants, the same change in velocity distribution is evident in Fig. 4d for larger $\overline{v}_\theta^{max}$.

Finally in Figs. 5 and 6, for two different time instants, the distribution in the numerical specimen of both r_c (Section 3.1) and porosity n is illustrated. Initially, r_c is not nil in all the domain, (Fig. 5a-b) and the material is behaving like a solid. The inner region stresses are larger than the external ones and the internal crown of the rheometer slightly compact. The outer region, due to the almost incompressibility of the fluid, ensuring a constant mean value of porosity, slightly dilates (Fig. 6a-b) to counterbalance the inner region compaction. At time instants c) and d), the material is fluid-like in the external crown (Fig. 5c and 5d), confirming what observed with reference to the velocity profiles of Fig. 4c-d. In the external crown, due to the material agitation and to the increase in T, the material experiences a further increase in porosity and specimen heterogeneity is magnified.

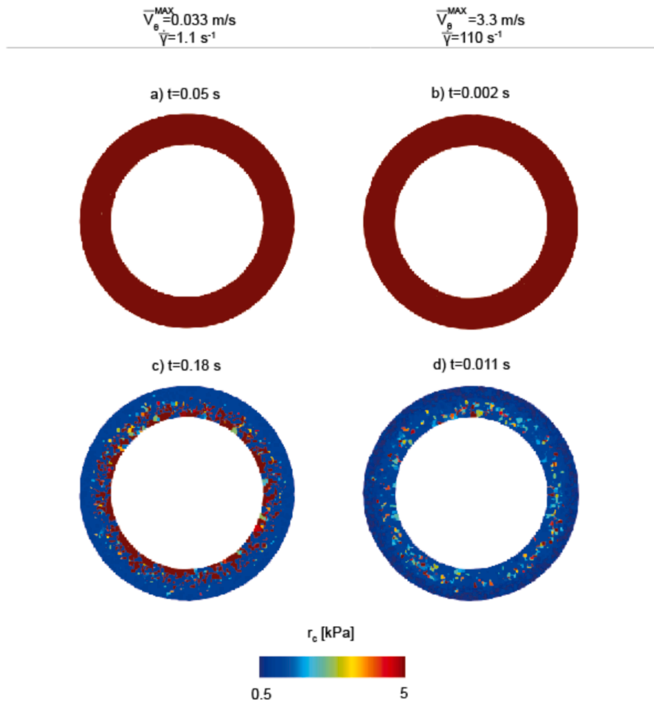

Fig. 5. Test 1 and 3: spatial distribution of isotropic hardening variable r_c for different instants of time.

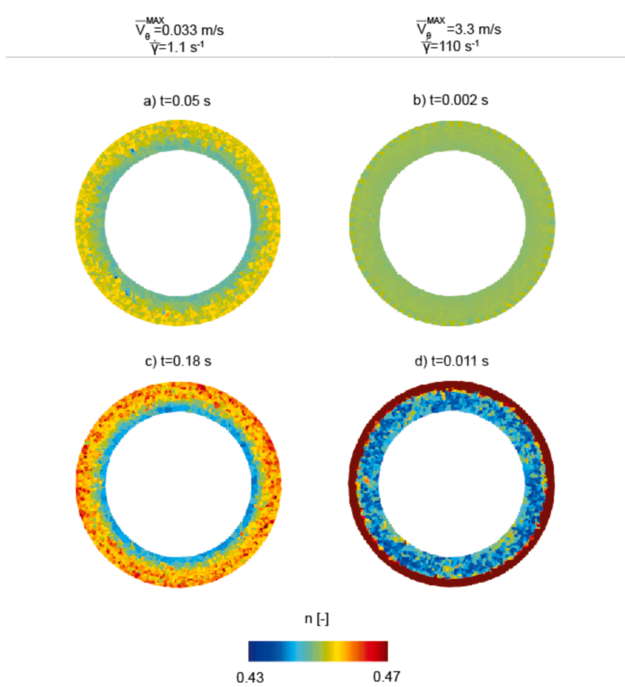

Fig. 6. Test 1 and 3: spatial distribution of porosity for different instants of time.

7. Conclusions

In this paper, the problem of numerically simulating regime transition processes in granular media is tackled. The authors introduce a new version of a multi regime model, already employed to reproduce the mechanical behaviour of dry granular specimens, suitable for taking the presence of water within the pores into consideration. Original is also the implementation of the model into a double-phase-double-point Material Point Method numerical code.

The constitutive model is based on a thermodynamic interpretation of the mechanisms governing at the micro-scale the interaction among grains and water and is tailored on mixture theories. According to the model, the regime transition is mainly governed by two scalar variables: the material porosity and the granular temperature (a measure this latter of the agitation state of the system). The model is inspired to kinetic theories of granular gasses and local critical state elastic-plasticity. In the new version proposed in this paper, the energy exchange between solid and liquid phases has been taken into account by introducing an additional coupling term in the energy balance equation. The role of energy balance equation is also crucial in the implementation of the model in Material Point Method code, since this latter also accounts for energy fluxes.

The role of strain rate in affecting the mechanical behaviour of granular materials is emphasized by simulating standard compression undrained triaxial tests performed on a loose sand specimen. When the material behaves like a solid, until effective mean pressure does not nullify, the deviatoric strain rate imposed does not modify the material response. On the contrary, at liquefaction, larger values of deviatoric strain rate are associated with larger values of stress deviator. When the deviatoric strain rate is sufficiently large, the mixture experiences the transition to Newtonian to Bagnoldian regime.

Finally, the authors discuss, by numerically simulating an undrained constant volume rheometer test, the uniformity/homogeneity of the specimen before and after liquefaction. The problem is tackled by using the material point method numerical code and by performing the same test at three different angular velocities. This particular test in employed to maintain a pore water pressure constant in the specimen, but to quantify the role of water in affecting the mechanical response of the material. The authors show that material liquefaction is associated with a marked non uniform distribution of porosity, velocity and shear strain rate.

CRediT authorship contribution statement

Pietro Marveggio: Writing – review & editing, Writing – original draft, Visualization, Software, Methodology, Investigation, Formal analysis, Data curation, Conceptualization. **Matteo Zerbi:** Writing – review & editing, Validation, Software, Investigation, Data curation, Conceptualization. **Claudio di Prisco:** Writing – review & editing, Visualization, Supervision, Methodology, Formal analysis, Conceptualization.

Declaration of competing interest

The authors declare that they have no known competing financial interests or personal relationships that could have appeared to influence the work reported in this paper.

Data availability

No data was used for the research described in the article.

References

Aifantis, E.C., 1992. On the role of gradients in the localization of deformation and fracture. Int. J. Eng. Sci. 30 (10), 1279–1299. https://doi.org/10.1016/0020-7225(92)90141-3.

Alaei, E., Marks, B., Einav, I., 2021. A hydrodynamic-plastic formulation for modelling sand using a minimal set of parameters. J. Mech. Phys. Solids 151, 104388. https://doi.org/10.1016/j.jmps.2021.104388.

Anura 3d., 2023. Software, ANURA3D Community.

Aranson, I.S., Tsimring, L.S., 2006. Patterns and collective behavior in granular media: Theoretical concepts. Rev. Mod. Phys. 78 (2), 641–692. https://doi.org/10.1103/RevModPhys.78.641.

Baumgarten, A.S., Kamrin, K., 2019. A general fluid–sediment mixture model and constitutive theory validated in many flow regimes. J. Fluid Mech. 861, 721–764. https://doi.org/10.1017/jfm.2018.914.
Berzi, D., Di Prisco, C.G., Vescovi, D., 2011. Constitutive relations for steady, dense granular flows. Phys. Rev. E 84 (3), 031301. https://doi.org/10.1103/PhysRevE.84.031301.
Berzi, D., Jenkins, J.T., 2015. Steady shearing flows of deformable, inelastic spheres. Soft Matter 11 (24), 4799–4808. https://doi.org/10.1039/C5SM00337G.
Bingham, E.C., 1922. Fluidity and Plasticity. Mcgraw-Hill Book Company Inc.
Boyer, F., Guazzelli, É., Pouliquen, O., 2011. Unifying Suspension and Granular Rheology. Phys. Rev. Lett. 107 (18), 188301 https://doi.org/10.1103/PhysRevLett.107.188301.
Calvetti, F., Emeriault, F., 1999. Interparticle forces distribution in granular materials: Link with the macroscopic behaviour. Mechanics of Cohesive-frictional Materials 4 (3), 247–279. https://doi.org/10.1002/(SICI)1099-1484(199905)4:3<247::AID-CFM62>3.0.CO;2-V.
Calvetti, F., Di Prisco, C., Redaelli, I., Sganzerla, A., Vairaktaris, E., 2019. Mechanical interpretation of dry granular masses impacting on rigid obstacles. Acta Geotech. 14 (5), 1289–1305. https://doi.org/10.1007/s11440-019-00831-9.
Campbell, C.S., 2006. Granular material flows – An overview. Powder Technol. 162 (3), 208–229. https://doi.org/10.1016/j.powtec.2005.12.008.
Chèvremont, W., Bodiguel, H., Chareyre, B., 2020. Lubricated contact model for numerical simulations of suspensions. Powder Technol. 372, 600–610. https://doi.org/10.1016/j.powtec.2020.06.001.
Chialvo, S., Sun, J., Sundaresan, S., 2012. Bridging the rheology of granular flows in three regimes. Phys. Rev. E 85 (2), 021305. https://doi.org/10.1103/PhysRevE.85.021305.
Clerc, A., Wautier, A., Bonelli, S., Nicot, F., 2021. Mesoscale inertial transition in granular materials. EPJ Web of Conferences 249, 10004. https://doi.org/10.1051/epjconf/202124910004.
Dafalias, Y.F., Manzari, M.T., 2004. Simple Plasticity Sand Model Accounting for Fabric Change Effects. J. Eng. Mech. 130 (6), 622–634. https://doi.org/10.1061/(ASCE)0733-9399(2004)130:6(622).
De Borst, R., Mühlhaus, H., 1992. Gradient-dependent plasticity: Formulation and algorithmic aspects. Int. J. Numer. Meth. Eng. 35 (3), 521–539. https://doi.org/10.1002/nme.1620350307.
di Prisco, C., Nova, R., Lanier, J., 1993. A Mixed Isotropic-Kinematic Hardening Constitutive Law for Sand. In: Modern Approaches to Plasticity. Elsevier, pp. 83–124. https://doi.org/10.1016/B978-0-444-89970-5.50010-8.
Ergun, S., 1952. Fluid Flow through Packed Columns. Chem. Eng. Prog. 89–95.
Fern, J., Rohe, A., Soga, K., Alonso (A c. Di), E., 2019. The Material Point Method for Geotechnical Engineering: A Practical Guide, (1a ed.). CRC Press. https://doi.org/10.1201/9780429028090.
Gajo, A., Muir Wood, D., 1999. A kinematic hardening constitutive model for sands: The multiaxial formulation. Int. J.for Numerical and Analytical Methods in Geomechanics 23 (9), 925–965. https://doi.org/10.1002/(SICI)1096-9853(19990810)23:9<925::AID-NAG19>3.0.CO;2-M.
Garzó, V., Dufty, J.W., 1999. Dense fluid transport for inelastic hard spheres. Phys. Rev. E 59 (5), 5895–5911. https://doi.org/10.1103/PhysRevE.59.5895.
Guo, X., Peng, C., Wu, W., Wang, Y., 2021. Unified constitutive model for granular–fluid mixture in quasi-static and dense flow regimes. Acta Geotech. 16 (3), 775–787. https://doi.org/10.1007/s11440-020-01044-1.
Hunt, M.L., Zenit, R., Campbell, C.S., Brennen, C.E., 2002. Revisiting the 1954 suspension experiments of R. A. Bagnold. *Journal of Fluid Mechanics* 452, 1–24. https://doi.org/10.1017/S0022112001006577.
Hutter, K., Jöhnk, K., 2004. Continuum Methods of Physical Modeling. Springer, Berlin Heidelberg. https://doi.org/10.1007/978-3-662-06402-3.
Jaeger, H.M., Nagel, S.R., Behringer, R.P., 1996. Granular solids, liquids, and gases. Rev. Mod. Phys. 68 (4), 1259–1273. https://doi.org/10.1103/RevModPhys.68.1259.
Jenkins, J.T., Savage, S.B., 1983. A theory for the rapid flow of identical, smooth, nearly elastic, spherical particles. J. Fluid Mech. 130 (1), 187. https://doi.org/10.1017/S0022112083001044.
Jop, P., Forterre, Y., Pouliquen, O., 2006. A constitutive law for dense granular flows. Nature 441 (7094), 727–730. https://doi.org/10.1038/nature04801.
Leonardi, A., Wittel, F.K., Mendoza, M., Herrmann, H.J., 2014. Coupled DEM-LBM method for the free-surface simulation of heterogeneous suspensions. Computational Particle Mechanics 1 (1), 3–13. https://doi.org/10.1007/s40571-014-0001-z.
Lun, C.K.K., 1991. Kinetic theory for granular flow of dense, slightly inelastic, slightly rough spheres. J. Fluid Mech. 233, 539–559. https://doi.org/10.1017/S0022112091000599.
Marveggio, P., Zerbi, M., Redaelli I. & Di Prisco, C. (Submitted). Granular material regime transitions during high energy impacts of dry flowing masses: MPM simulations with a multi-regime constitutive model.
Marveggio, P., Zerbi, M., Di Prisco, C., 2023. Modelling Phase Transition in Saturated Granular Materials in MPM. In: Ferrari, A., Rosone, M., Ziccarelli, M., Gottardi (A c. Di), G. (Eds.), Geotechnical Engineering in the Digital and Technological Innovation Era. Springer Nature, Switzerland, pp. 452–459. https://doi.org/10.1007/978-3-031-34761-0_55.
Marveggio, P., Redaelli, I., di Prisco, C., 2022. Phase transition in monodisperse granular materials: How to model it by using a strain hardening visco-elastic-plastic constitutive relationship. Int. J.for Numerical and Analytical Methods in Geomechanics 46 (13), 2415–2445. https://doi.org/10.1002/nag.3412.
MiDi, G.D.R., 2004. On dense granular flows. The European Physical Journal E 14 (4), 341–365. https://doi.org/10.1140/epje/i2003-10153-0.
Ness, C., Sun, J., 2015. Flow regime transitions in dense non-Brownian suspensions: Rheology, microstructural characterization, and constitutive modeling. Phys. Rev. E 91 (1), 012201. https://doi.org/10.1103/PhysRevE.91.012201.
Nova, R., 1988. Sinfonietta classica: An exercise on classical soil modelling. Proc. Symp. Constitutive Eq. for Granular Non-Cohesive Soils 501–520.
Redaelli, I., di Prisco, C., Vescovi, D., 2016. A visco-elasto-plastic model for granular materials under simple shear conditions: A Visco-Elasto-Plastic Model for Granular Materials. Int. J. Numer. Anal. Meth. Geomech. 40 (1), 80–104. https://doi.org/10.1002/nag.2391.
Redaelli, I., Di Prisco, C., 2019. Three dimensional steady-state locus for dry monodisperse granular materials: DEM numerical results and theoretical modelling. Int. J. Numer. Anal. Meth. Geomech. 43 (16), 2525–2550. https://doi.org/10.1002/nag.2985.
Redaelli, I., di Prisco, C., 2021. DEM numerical tests on dry granular specimens: The role of strain rate under evolving/unsteady conditions. Granul. Matter 23 (2), 39. https://doi.org/10.1007/s10035-021-01091-9.
Redaelli, I., Marveggio, P., Di Prisco, C., 2021. Three-Dimensional Constitutive Model for Dry Granular Materials Under Different Flow Regimes. In: Barla, M., Di Donna, A., Sterpi (A c. Di), D. (Eds.), Challenges and Innovations in Geomechanics, 125. Springer International Publishing, pp. 548–555. https://doi.org/10.1007/978-3-030-64514-4_55.
Savage, S.B., 1998. Analyses of slow high-concentration flows of granular materials. J. Fluid Mech. 377, 1–26. https://doi.org/10.1017/S0022112098002936.
Soga, K., Alonso, E., Yerro, A., Kumar, K., Bandara, S., 2016. Trends in large-deformation analysis of landslide mass movements with particular emphasis on the material point method. Géotechnique 66 (3), 248–273. https://doi.org/10.1680/jgeot.15.LM.005.
Truesdell, C., Toupin, R., 1960. The Classical Field Theories. In: Flügge (A c. Di), S. (Ed.), Principles of Classical Mechanics and Field Theory / Prinzipien der Klassischen Mechanik und Feldtheorie. Springer, Berlin Heidelberg, pp. 226–858. https://doi.org/10.1007/978-3-642-45943-6_2.
Trulsson, M., Andreotti, B., Claudin, P., 2012. Transition from the Viscous to Inertial Regime in Dense Suspensions. Phys. Rev. Lett. 109 (11), 118305 https://doi.org/10.1103/PhysRevLett.109.118305.
Tsuji, Y., Kawaguchi, T., Tanaka, T., 1993. Discrete particle simulation of two-dimensional fluidized bed. Powder Technol. 77 (1), 79–87. https://doi.org/10.1016/0032-5910(93)85010-7.
Vescovi, D., di Prisco, C., Berzi, D., 2013. From solid to granular gases: The steady state for granular materials. Int. J. Numer. Anal. Meth. Geomech. 37 (17), 2937–2951. https://doi.org/10.1002/nag.2169.
Vescovi, D., Marveggio, P., Di Prisco, C.G., 2020. Saturated granular flows: Constitutive modelling under steady simple shear conditions. Géotechnique 70 (7), 608–620. https://doi.org/10.1680/jgeot.19.P.023.
Wang, S., Guo, S., Gao, J., Lan, X., Dong, Q., Li, X., 2012. Simulation of flow behavior of liquid and particles in a liquid–solid fluidized bed. Powder Technol. 224, 365–373. https://doi.org/10.1016/j.powtec.2012.03.022.
Wilson, P., Wüchner, R., Fernando, D., 2021. Distillation of the material point method cell crossing error leading to a novel quadrature-based C 0 remedy. Int. J. Numer. Meth. Eng. 122 (6), 1513–1537. https://doi.org/10.1002/nme.6588.